

On coherent vortical structures in wave breaking

Alessandro Iafrati, Simone Di Giorgio and Sergio Pirozzoli

CNR-INM, Istituto di Ingegneria del Mare, Via di Vallerano 139, Rome, 00128, Italy
alessandro.iafrati@inm.cnr.it

1 INTRODUCTION

The flow generated by the breaking of a steep free-surface wave in a periodic domain is simulated numerically with a two-fluids Navier-Stokes solver. The model employs a Volume-of-Fluid (VOF) technique to distinguish the two fluids. The advection of the VOF function is carried out by using novel schemes based on a tailored total-variation-diminishing (TVD) limiter. The numerical solver is characterized by a low numerical dissipation, thanks to the use of a scheme that guarantees energy conservation in the discrete form. Both two- and three-dimensional simulations have been performed. Particular attention is paid to the analysis of the mechanisms responsible for the energy dissipation during the breaking. To this purpose, coherent vortical structures, such as vortex tubes and vortex sheets, are identified. A rather strong correlation between the vortical structures generated as a consequence of the air entrainment and of the bubble fragmentation process and the energy dissipation is found both in the mixing zone and in the pure water domain, where the coherent structures propagate as a consequence of the downward transport. Notably, it is found that the dissipation is primarily identified by the vortex sheets whereas the vortex tubes govern mainly the intermittency.

2 COMPUTATIONAL SETUP

The two-phase flow of air and water taking place during the breaking of free surface wave is numerically simulated by a Navier-Stokes solver for a single incompressible fluid with variable physical properties across the interface. The fluids are assumed to be immiscible, and the interface is implicitly tracked by means of an indicator function, i.e. the VOF function. Hereafter, the subscripts 1 and 2 are used to denote water and air, respectively. The governing equations in nondimensional form are

$$\nabla \cdot \mathbf{u} = 0, \quad (1)$$

$$\frac{\partial \mathbf{u}}{\partial t} + \nabla \cdot (\mathbf{u}\mathbf{u}) = \frac{1}{\rho} \left[-\nabla p + \frac{1}{Re} \nabla \cdot (\mu (\nabla \mathbf{u} + \nabla \mathbf{u}^T)) + \frac{1}{We} \mathbf{f}_\sigma \right] - \frac{1}{Fr} \mathbf{j}, \quad (2)$$

where \mathbf{u} is the fluid velocity, p is the pressure, ρ is the local density, μ is the local value of the dynamic viscosity, and \mathbf{j} is the unit vector oriented upwards. Here, lengths are made nondimensional with respect to the fundamental wavelength (λ), velocities by $\tilde{U} = (g\lambda)^{1/2}$ (with g the gravity acceleration), density and viscosity with the respective values in water, pressure by $\rho_1 \tilde{U}^2$. Although surface tension only acts at the interface, its effects are modelled as a distributed volumetric force $\mathbf{f}_\sigma = \mathbf{f}_\sigma(\mathbf{x}, t)$, with

$$\mathbf{f}_\sigma = k\delta(\mathbf{x} - \mathbf{x}_s) \mathbf{n}, \quad (3)$$

where k is the local curvature of the interface between the two fluids \mathbf{n} is the unit normal of the interface, and δ is the Dirac function which localizes the force at interface points, \mathbf{x}_s [1]. In equation (2), the Reynolds, Weber and Froude numbers are defined as $Re = \frac{\tilde{U}\lambda\rho_1}{\mu_1}$, $We = \frac{\rho_1\tilde{U}^2\lambda}{\sigma}$, and $Fr = \frac{\tilde{U}^2}{g\lambda}$, where σ is the surface tension coefficient, here assumed to be constant.

The Navier-Stokes equations are solved with a classical projection method [2]. Adams-Bashforth scheme is used for the time integration of the convective terms and for the off-diagonal part of the viscous terms, and the Crank-Nicolson scheme for the diagonal diffusion terms. A centered, second-order, finite-difference scheme in a staggered grid layout is adopted for spatial derivatives[3]. The continuum surface force method [4], is used to determine the equivalent local body force. The interface curvature is evaluated through a modified version of the height function technique [5].

The advection of the interface is carried out by means of an algebraic VOF method [6]. After computing the passive tracer C , density and viscosity are determined from $(\rho, \mu) = C + (\rho, \mu)_2/(\rho, \mu)_1(1 - C)$. More details regarding the multiphase solver can be found in [7].

3 SIMULATION CONDITIONS

The model is applied to simulate the breaking generated by a steep wave in a periodic domain. The initial free-surface elevation $\eta(x, z)$ is assigned as in [8], that is

$$\eta(x, z) = \frac{\epsilon}{2\pi} \left(\cos(k(x - r(z)\Delta x)) + \frac{1}{2}\epsilon \cos(2k(x - r(z)\Delta x)) + \frac{3}{8}\epsilon^2 \cos(3k(x - r(z)\Delta x)) \right), \quad (4)$$

where $\epsilon = 0.5$ is the initial wave steepness, and $k = 2\pi$ is the fundamental wavenumber. A small perturbation is introduced in the initial wave profile in the form of a random shift by a fraction ($0 \leq r(z) \leq 1$) of the grid cell size. No-slip boundary conditions are assigned at the top and bottom boundaries. Density and viscosity ratios are assumed to be those of water/air case, i.e. $\rho_1/\rho_2 = 800$, and $\mu_1/\mu_2 = 55$ and the surface tension coefficient is chosen as 0.072 N/m. Simulations are conducted by using $We = \frac{\rho_1 g \lambda^2}{\sigma} = 12262.5$ and $Re = \frac{\rho_1 g^{1/2} \lambda^{3/2}}{\mu_1} = 10000$, and 40000. The computational domain is one fundamental wavelength long (streamwise direction), two fundamental wavelength high (vertical direction) and, for three-dimensional simulations, one-half fundamental wavelength wide (spanwise direction). Assuming $\lambda = 30\text{cm}$, the resulting grid spacing in the well-resolved zone is about 0.3 mm in the fine-mesh simulations.

4 COHERENT VORTICAL STRUCTURES AND DISSIPATION

In [8] it was shown that the bubble fragmentation process enhances the energy dissipation. Here, the mechanisms are investigated more in depth. To this purpose, the coherent vortical structures generated during the breaking phenomenon are identified. More specifically, here vortex tubes and vortex sheets are examined: the former are correlated with elongated vortices whereas the second are correlated with shears [7]). Fig. 1 shows two different views of the simulation at $Re = 40000$ at a given time instant, with vortex-tubes drawn in yellow

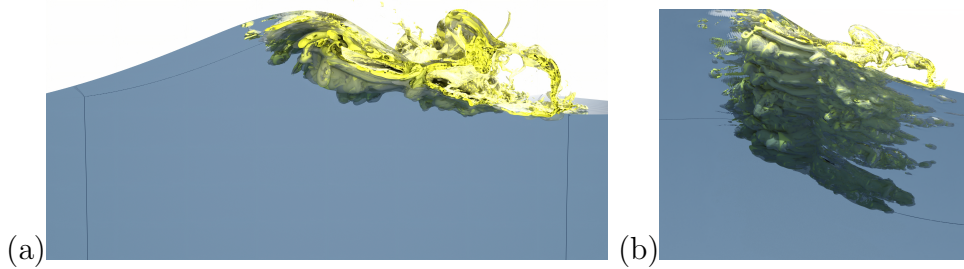


Figure 1: Underwater vortical structures generated during the breaking: vortex-tubes and vortex-sheets are drawn in yellow and gray, respectively.

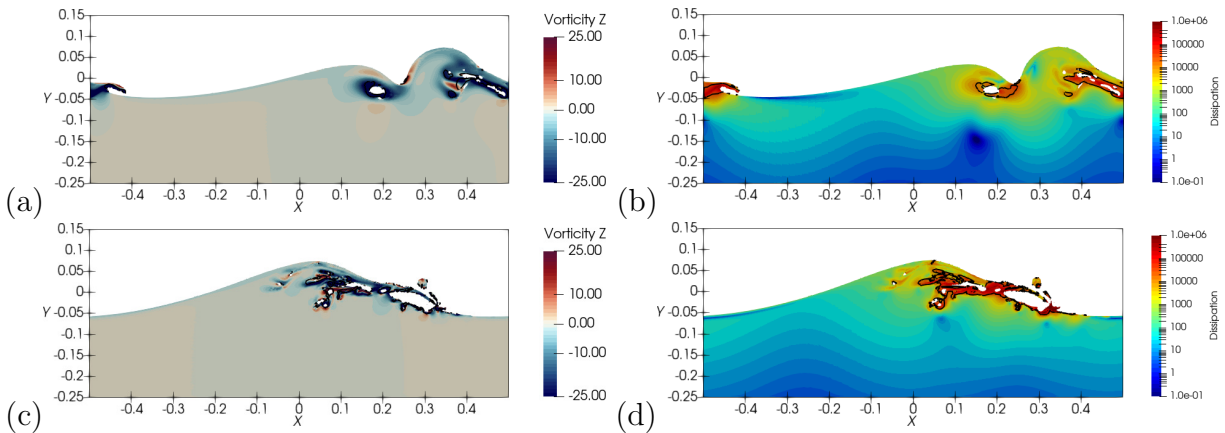


Figure 2: Longitudinal sections of the solutions computed at $Re = 10000$ (top) and $Re = 40000$ (bottom). The coloured contours denote the local values of the normal-to-plane vorticity components (left), and the local dissipation rate (right). The black solid lines in left and right figures denote the vortex-tube and vortex-sheet iso-lines, respectively. Note that the solutions in the water domain is shown only.

and vortex-sheets drawn in gray. It can be seen that, as a consequence of the entrainment of the large air cavity during the breaking and of the subsequent bubble fragmentation, large velocity gradients develops within the bubble cloud, which are reflected into the vortical structures. In order to highlight the connections between air entrainment and viscous dissipation with vortical structures, in fig. 2, slices taken in the longitudinal symmetry plane are drawn. The results display a very close correlation between viscous dissipation and the vortex sheet indicator, at both Reynolds numbers. Also, it is worth noticing that viscous dissipation is not confined about the free surface, but it is spread within the bubble cloud. Within the high-dissipation regions, marked by the vortex sheet indicator, vortex tubes also form in zones with high vorticity. In order to retrieve more quantitative information about the statistics among the various indicators, vertical profiles of their averages in the longitudinal and spanwise directions are displayed in fig. 3. For both Reynolds numbers, the vorticity and maximum dissipation is mainly concentrated in the mixing region. It is clear that the concentration of high vorticity, vortical structures and dissipation happens primarily where the fragmentation and bubbles productions phenomena take place. However, the graphs shows that the viscous dissipation and the vortex-sheets are still significant in the pure water region, whereas the vortex-tubes vanish suddenly when leaving the mixing zone.

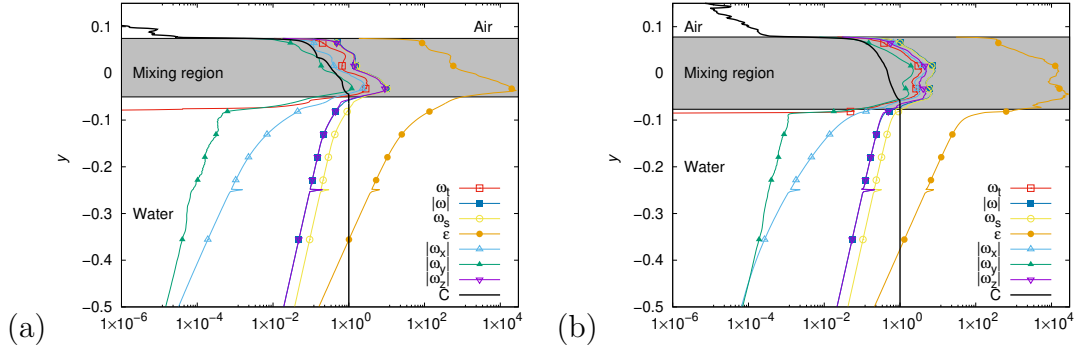


Figure 3: Vertical profiles of horizontal (spanwise and streamwise) averages of viscous dissipation (ϵ), vorticity modulus ($|\omega|$), streamwise vorticity ($|\omega_x|$), vertical vorticity ($|\omega_y|$), spanwise vorticity ($|\omega_z|$), vorticity-like variable for vortex tubes (ω_t), vorticity-like variable for vortex sheet (ω_s), and mean volume fraction (\bar{C}), at $Re = 10000$ (a) and $Re = 40000$ (b). The shaded area denotes the mixing region ($0.001 < \bar{C} < 0.999$)

The above results agrees with what is generally found, i.e. that dissipation is primarily associated with vortex sheets, whereas vortex tubes, being generated upon sheets roll-up [9], are much less relevant.

REFERENCES

- [1] Tryggvason, G., Scardovelli, R., and Zaleski, S. 2011. *Direct Numerical Simulations of Gas-Liquid Multiphase Flows*. Cambridge University Press.
- [2] Chorin, A. J. 1968. *Numerical Solution of the Navier-Stokes Equations*. *Math. Comp.* 22, 745 – 762.
- [3] Harlow, F. H., and Welch, J. E. 1965. *Numerical calculation of time-dependent viscous incompressible flow of fluid with free surface*. *Phys. Fluids* 8(12), 2182–2189.
- [4] Brackbill, J. U., Kothe, D. B., and Zemach, C. 1992. *A continuum method for modeling surface tension*. *J. Comput. Phys.* 100(2), 335–354.
- [5] Popinet, S. 2009. *An accurate adaptive solver for surface-tension-driven interfacial flows*. *J. Comput. Phys.* 228(16), 5838–5866.
- [6] Pirozzoli, S., Di Giorgio, S., and Iafrafi, A. 2019. *On algebraic TVD-VOF methods for tracking material interfaces*. *Comput. Fluids* 189, 73–81.
- [7] Di Giorgio, S., Pirozzoli, S., and Iafrafi, A. 2022. *On coherent vortical structures in wave breaking*. *Journal of Fluid Mechanics* 947, A44.
- [8] Iafrafi, A. 2009. *Numerical study of the effects of the breaking intensity on wave breaking flows*. *J. Fluid Mech.* 622, 371–411.
- [9] Kawahara, G. 2005. *Energy dissipation in spiral vortex layers wrapped around a straight vortex tube*. *Phys. Fluids* 17(5), 055111.